Supplementary Materials for

Global perturbation of stratospheric water and aerosol burden by Hunga eruption

Sergey Khaykin*, Aurelien Podglajen, Felix Ploeger, Jens-Uwe Grooß, Florent Tence, Slimane Bekki, Konstantin Khlopenkov, Kristopher Bedka, Landon Rieger, Alexandre Baron, Sophie Godin-Beekmann, Bernard Legras, Pasquale Sellitto, Tetsu Sakai, John Barnes, Osamu Uchino, Isamu Morino, Tomohiro Nagai, Robin Wing, Gerd Baumgarten, Michael Gerding, Valentin Duflot, Guillaume Payen, Julien Jumelet, Richard Querel, Ben Liley, Adam Bourassa, Benjamin Clouser, Artem Feofilov, Alain Hauchecorne, François Ravetta

*Correspondence to: sergey.khaykin@latmos.ipsl.fr

This PDF file includes:

Other Supplementary Materials for this manuscript include the following:

Data set	Type	Parameters
GOES-17 and Himawari-8	Geostationary satellites	Eruptive cloud top height
FORMOSAT-7 COSMIC-2	Radio occultation satellites	Vertical profiles of H_2O and refractivity
Aura MLS	Satellite microwave limb sounder	Vertical profiles of H_2O and geopotential height
Suomi NPP OMPS-LP	Satellite limb-scattering profiler	Vertical profiles of aerosol extinction
CALIPSO CALIOP	Satellite cloud/aerosol lidar	Vertical profiles of aerosol backscatter and depolarization at 532 nm
SCISAT ACE-FTS	Satellite solar occultation spectrometer	Vertical profiles of HDO and H_2O (water isotopic ratio)
ISS SAGE III	Satellite solar occultation spectrometer	Vertical profiles of aerosol extinction and water vapour
Aeolus ALADIN	Satellite wind/aerosol lidar	Vertical profiles of aerosol backscatter 355 nm
Vaisala RS41 meteorological radiosounding	Regular upper-air soundings	Vertical profiles of water vapour and relative humidity
Stratospheric aerosol lidars (8 stations)	Ground-based lidars	Vertical profiles of aerosol backscatter at 532 nm
GloSSAC	Merged satellite record	Vertical profiles of aerosol extinction
CLaMS	Chemistry-transport model	Vertical profiles of H_2O
ECMWF IFS	Operational analysis	Meteorological fields

Supplementary Table S1. Overview of data sets involved in this study with brief information on their type and parameters exploited.

Supplementary Notes

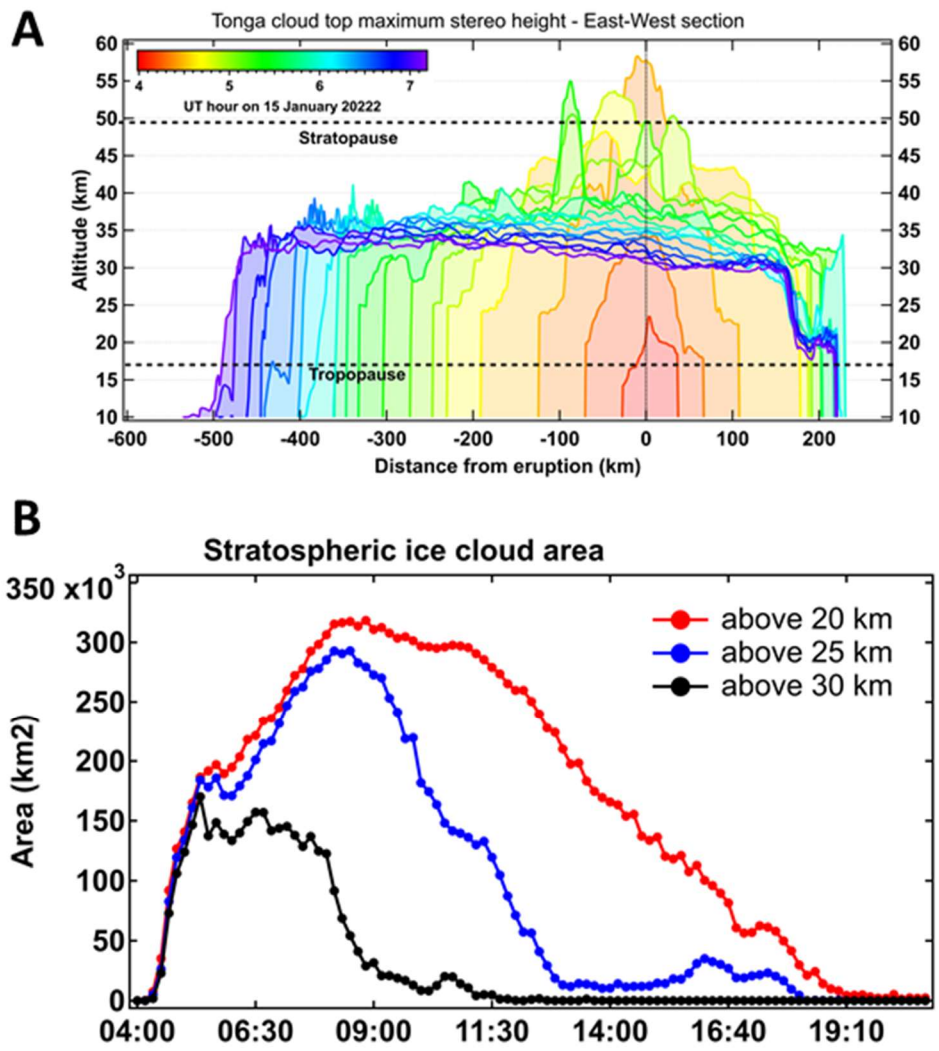

Figure S1. Evolution of the Hunga ice cloud on the day of eruption (15 January 2022) from stereoscopic analysis of GOES-17 and Himawari-8 satellite imagers. (a) East-West sections of maximum CTH color-coded by time; (b) Total area of the cloud at different altitude levels.

Supplementary notes S.I. COSMIC-2 observations on the day of eruption

The stratospheric water vapor profiles retrieved from COSMIC-2 GNSS radio occultations and ECMWF temperature exhibit unprecedented water vapor values in the observational record (more than 14,000 ppmv at 33 km, Fig. 1d) but remain of the order of the physical limit of ice saturation (Fig. S3), giving confidence in the procedure despite its crudeness. This data can be considered observational evidence for hydration of the stratosphere to ice saturation up to 33 km, and is also consistent with the geostationary RGB imagery pointing to ice formation in the early evolution of the plume. Extrapolating the early water vapor columns to the whole umbrella cloud (area of 150,000 km2, see Fig. S1) and setting unphysical values to background (if negative) or saturation (if above saturation), we obtain estimates for the stratospheric water injection of 76-140 Tg, respectively. This is assuming all water is found as vapor, ice having either fallen out or sublimated. A similar estimate (100 Tg) can be obtained assuming ECMWF temperature and water saturation up to 33 km (the top altitude of the umbrella) and background levels (5 ppmv) above.

Later profiles already point to a significant subsidence of the initial plume and its dilution as it is carried away by the sheared flow. Beyond January 15th, a persistent refractivity anomaly >2% can be followed traveling West together with the plume to the end of January at least, consistent with radiosondes indicating water vapor amounting > 1,000 ppmv for the first overpass over Australia (Jan 17-19), and > 100 ppmv for the second.

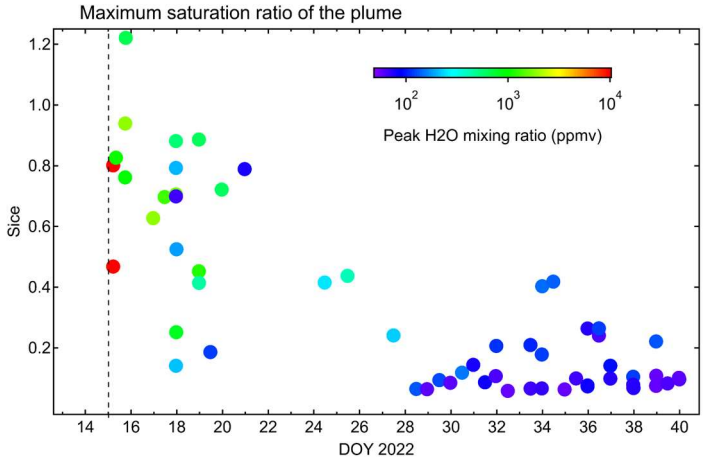

Figure S2. Evolution of the maximum ice saturation ratio (Sice) of the stratospheric hydrated plumes from COSMIC-2 water vapour retrieval and radiosoundings.

Supplementary notes S.II. CLaMS simulation and comparison with MLS observations

Since the location of the detected plume does significantly change during one day, MLS observations over an analysis period are advected forward or backward in time in order to map all the observations of that time window on the same central time. With this trajectory correction to the position of the MLS observations within one period, typically one calendar day, the position

of the observation is supposed to be where the sampled air mass would have been at a given synoptic time, typically 12:00 UTC on that calendar day. These locations were determined using CLaMS backward and forward trajectories. The data at these locations are then directly comparable with the CLaMS model output at the same synoptic time. Based on this approach, synoptic maps of MLS water vapor were constructed. For a given regular grid of 1 degrees latitude and 3 degrees longitude, all so-defined synoptic observations were averaged to the grid points using a 1/r weighting factor for the distance r to the corresponding grid point.

As the existence of data gaps in MLS water vapor observations, particularly around the date of the eruption, causes the largest uncertainty in the model simulations, we carried out sensitivity simulations using both filtered and unfiltered MLS water vapor data (by applying/ignoring quality flag screening). Comparison of the simulated water vapor plume with the MLS observations after the eruption shows that initializing with unfiltered MLS data results in best agreement, likely related to the overlap of water vapor and sulphuric oxide spectral bands causing an erroneous filtering of large parts of the water vapor plume [1]. Therefore, the CLaMS simulation results for the Hunga perturbation shown in the paper are based on initialization with unfiltered MLS version 5 data on 18 January. Additional sensitivity simulations have been carried out using water vapor fields initialized on different days (17th, 19th, 25th of January), with gridding MLS observations onto a coarser 2x6 degree latitude-longitude grid, and also using the previous MLS data version 4. The conclusions of this paper are largely insensitive to these choices, however, the exact values of the simulated water vapor anomaly depend on the details of initialization. The missing data in MLS observations in regions of the volcanic plume on days close to the eruption, together with the missing heating rates due to the excess moisture in the plume [2], likely causes the largest uncertainty in the simulations. Initializing the simulation on a later date (e.g. 25th versus 18th January) results in a stronger simulated water vapor anomaly by lowering the effect of underestimation of the initial plume and reduces differences in the global mass perturbation between model and observations.

Figure S3 shows good agreement between the simulated and observed water vapor distribution following the eruption. The figure shows the plume evolution at 21 hPa level for better comparability with the rest of the paper, but note that the agreement between the simulation and observations is even better at levels above (e.g. 10 hPa), and somewhat worse at levels below (e.g. 68 hPa). During the first days after the eruption, the model represents the westward transport and distortion of the water vapor plume well (Fig. S3, until 1 February). In the following weeks there is evidence for a slightly too slow westward transport in the model (around mid-February). Also, the small-scale structures are better conserved in the simulated water vapor field compared to the MLS observations, potentially related to slightly underestimated mixing in the model or to the effect of the satellite averaging kernel smearing out small-scale structures. However, overall there is good agreement between the plume transport in the model simulation and in MLS observations from mid-January until March, providing confidence that the model reliably simulates the evolution of the stratospheric water vapor distribution after the Tonga eruption.

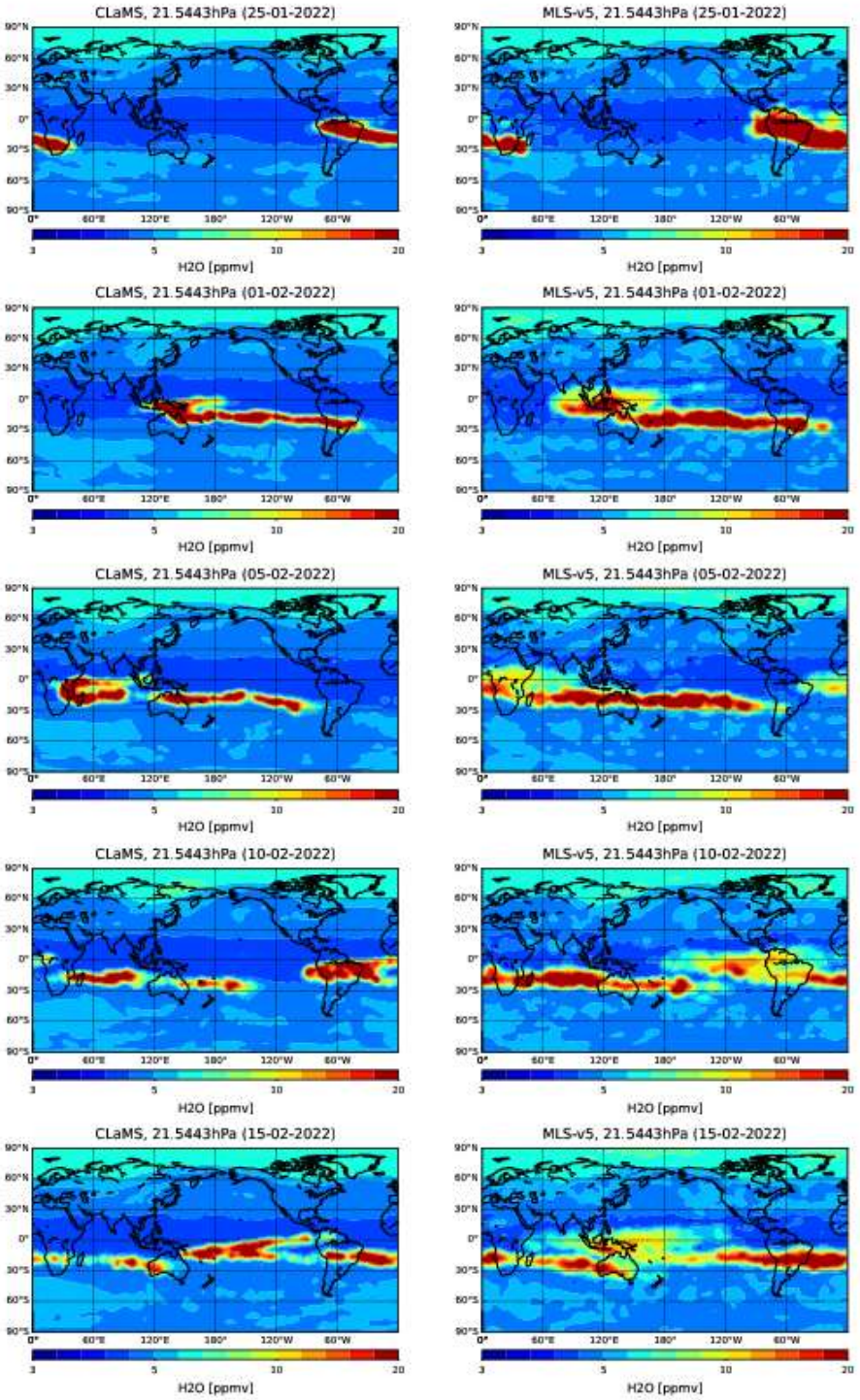

Figure S3. Comparison of CLaMS simulation and MLS observations of hydrated plume evolution. Maps of water vapor at 21 hPa from ClaMS model simulation (left) and MLS satellite observations (right) on selected days after the Tonga eruption (from top to bottom: 25.1., 1.2., 5.2., 10.2., 15.2.2022). The model water vapor field had been initialized with MLS values on 18 January 2022 (see text).

Supplementary notes S.III. Lidar first detections of Hunga aerosol plumes

Ground-based lidars at various locations across the globe operating at 532 nm wavelength were used in this study to verify and support the OMPS-derived meridional dispersion of the Hunga aerosols. The description of the measurement stations and lidar instruments is provided in Supplementary methods of this document.

Figure S5a shows the evolution of aerosol plume altitude as a function of latitude and time derived from OMPS-LP extinction ratio (ER) anomalies ER>3 (675 nm). The altitude of the plume corresponds to the mean altitude of the ER peak in each time-latitude bin, aggregating 50 - 80 individual OMPS-LP profiles. The first detections of Hunga stratospheric aerosol layers by lidars are marked as black open squares with altitude-dependent color meshing. The aerosol plumes are detected as local maxima in scattering ratio (SR) exceeding 1.2 at 532 nm. Note that Fig. S5a shows only the first unambiguous lidar detections of Hunga plumes, after which the stratospheric aerosol layers were omnipresent above each station (not shown). The altitude of the lidar aerosol layers may not necessarily match the satellite-derived plume altitude since the latter is obtained by aggregating many individual measurements within the given latitude band.

The first lidar station to sample the Hunga plume is the Atmospheric Physics Observatory of La Réunion (OPAR), which is located at the same latitude and downwind from the volcano given the easterly flow throughout the tropical stratosphere at that time. The first lidar acquisition after the eruption took place on 19 January (i.e. D+4) and sampled an aerosol layer extending between 33 - 37 km altitude (Fig. 5b), which to our knowledge is the highest-level aerosol plume ever observed by ground-based lidars. A much more intense aerosol plume between 27 - 30 km (the bulk layer) was overpassing above La Reunion two days later (D+6) and the lidar sounding showed the peak SR of 280 (Fig. S5b) and the AOD of the plume reaching 532 nm [3].

The second station to sample the Hunga plumes was Lauder, New Zealand (45° S), which reported a layer of spherical particles (i.e. sulfates, as inferred from the depolarization) with peak SR of 1.28 between 18-20 km altitude on 8 February (Fig. S5c), that is three weeks after the eruption. We note that OMPS-LP data suggest further quasi-isentropic transport towards the Southern pole (with the altitude descending along the isentropic surface, see Fig. 4B of the main paper), and this transport is captured by the lidar at the Antarctic Dumont d'Urville (67° S) station reporting a thin layer at 13.5 km altitude with peak SR of 1.22 (Fig. 5c).

While it took the first Hunga plumes only 10 days to cross the equator (Fig. 5a), the first lidar detection in the Northern hemisphere took place on 1 March at Mauna Loa observatory (Hawai, 20° N), that is about 6 weeks. The lidar reported a layer with peak SR of 1.34 at 24.5 km (Fig. 5d). By the end of March, the Hunga plumes have been subject to further northward transport and the first lidar detection in the Northern subtropics took place at the Japanese Tsukuba station (36° N), reporting a non-depolarizing layer of sulfates between 23 - 25 km with the peak SR of 1.7.

The further transport of Hunga aerosols towards the North pole, as suggested by OMPS-LP measurements, is confirmed by lidar detection at Kuhlungsborn, Germany (54° N) on 28 April, reporting a layer at 22 km altitude (Fig. 5g) in agreement with the satellite data showing limited transport of aerosols to the Northern mid and high latitudes. In early June, an aerosol layer was

detected at the Arctic Alomar station (69° N) in Norway (Fig. 5h). Interestingly, the first detection of Hunga aerosol at Haute Provence observatory (43° N) took place only on 3 June (Fig. 5k), although the Hunga aerosols were present at the northern midlatitude already since late April as suggested by other lidars.

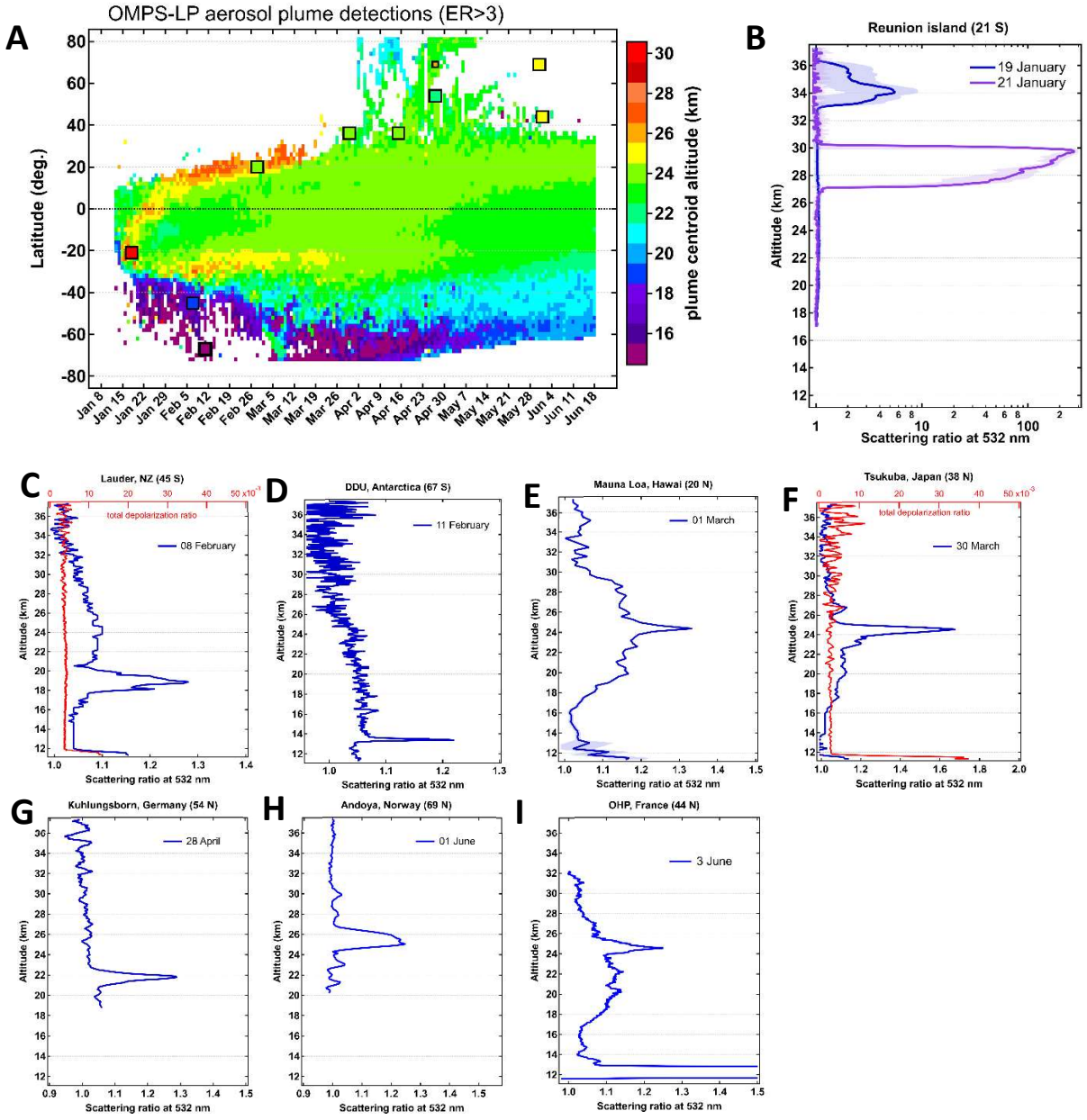

Figure S4. First detections of Hunga aerosol plumes by satellite and ground-based observations. (A) Time-latitude evolution of the altitude of aerosol layers detected using extinction ratio threshold ER>3 from OMPS-LP data at 675 nm. (B) scattering ratio profiles of the first Hunga plume measurements by lidar at La Reunion, note the log-scale and peak value of 280. (C - I) First detections of Hunga plumes at various stations. Depolarization ratio profiles are shown in red for Lauder and Tsukuba stations.

Supplementary notes S.IV. Stratospheric water vapour mass calculation

The water vapour mass estimation is based on the MLS-Aura v4.2 and v5 mixing ratio measurements. These measurements are considered between 100 hPa and 1 hPa, which corresponds roughly to 15 and 45 km altitude respectively. For the considered layer, the MLS data quality documents mention a precision between 4% and 15% for version 4.2 and between 5% and 7% for version 5. The data screening guidelines given by these documents were not considered here as they reject high H2O mixing ratios corresponding to the event studied here [1].

To estimate the total stratospheric water vapour mass between 100 hPa and 1 hPa, the globe was divided in 18 latitudinal bands of 10° width each. Inside each band, the mixing ratio profiles were averaged daily, then converted to a total number of H2O molecules between the given pressure levels boundaries, and then converted to a H2O mass value.

In each latitudinal band, the mixing ratio values are converted to water vapour partial column between 100 hPa and 1 hPa. *Xp* is the water vapour mixing ratio at the pressure *p*, and *Xcol* is the vapour vapour mixing ratio of the column between 100 hPa and 1 hPa. The -1/2 and +1/2 indices in the pressure scale represent the boundaries of each vertical layer considered around the MLS pressure scale.

$$X_{col} = \frac{[H2O]}{[air]} = \frac{\sum_{p=100hPa}^{1hPa} X_p \frac{P_{p-\frac{1}{2}} - P_{p+\frac{1}{2}}}{gM_{air}}}{\sum_{p=100hPa}^{1hPa} \frac{P_{p-\frac{1}{2}} - P_{p+\frac{1}{2}}}{gM_{air}}}$$

The number of water vapour molecules in the domain considered is given by the following formula, with Nair the number of air molecules in the domain, NA the Avogadro number, S the surface area of the domain:

$$N_{H2O} = X_{col} N_{air} = X_{col} S N_A \frac{P_{bottom-\frac{1}{2}} - P_{top+\frac{1}{2}}}{gM_{air}}$$

And finally, the mass of water vapour in the domain is calculated:

$$m_{H2O} = \frac{M_{H2O} N_{H2O}}{N_A} = M_{H2O} S \sum_{p=100hPa}^{1hPa} X_p \frac{P_{p-\frac{1}{2}} - P_{p+\frac{1}{2}}}{gM_{air}}$$

Finally, the stratospheric H2O mass is obtained as the sum of the masses calculated for each latitudinal band. The error bars on the mass of injection are estimated by combining accuracies on the measurements and the mean standard deviations over 20-day periods before and after the sharp increase.

Figure S6 shows the change of stratospheric H2O mass following the eruption estimated using MLS v4.2 and V.5 data. The V.5 data provides an estimate of 119±6 Tg or 7.9% of the pre-eruption stratospheric H2O mass. The V.4.2 data provides a larger estimate of 137±7 Tg (8.1%), which is in good agreement with a similarly obtained estimate of 139 ±8 Tg (8.9%) [4] albeit somewhat smaller than V.4.2-based estimate of 146±5 Tg (10%) [1]

We note that the absolute value of the injected H2O mass is sensitive to the vertical layer considered. In particular, using 380 K potential temperature level as the low boundary of the

stratospheric layer, we obtain 135±6 Tg using MLS V.5 or 146±5 Tg (9%) or 157±7 Tg (9.2%) using MLS V.4. Note though that while the absolute values vary from 119 to 157 Tg, the relative mass perturbation only varies between 7.9% - 9.2%.

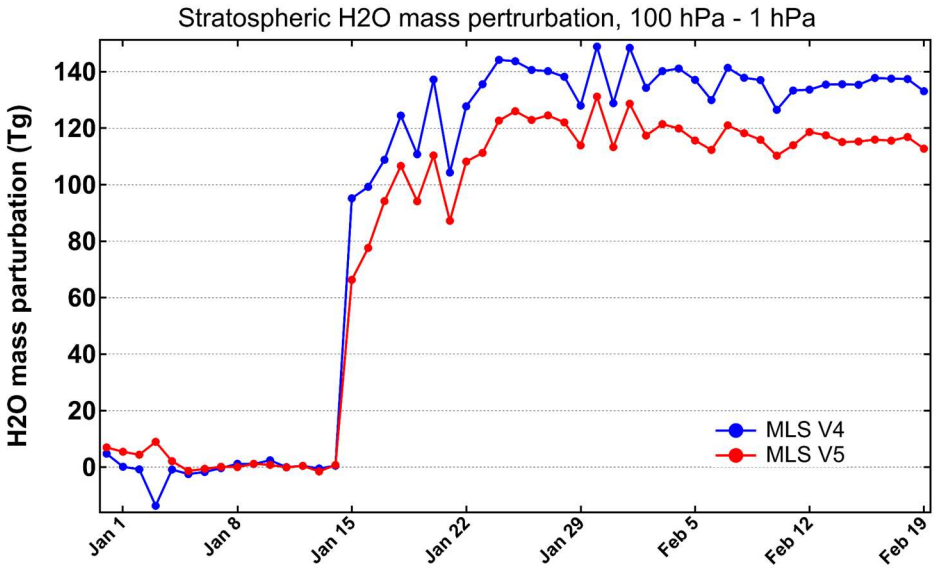

Figure S5. Hunga-induced change in the total mass of stratospheric water vapour between 100 hPa - 1 hPa pressure levels using MLS V4 and V5 data (see text for details)**.**

Supplementary notes S.V. Particle growth and sedimentation

Particle size is retrieved from SAGE III/ISS by fitting the extinction spectrum from 384 to 1540 nm using a unimodal lognormal particle size distribution. Typically, particles in the stratosphere are composed primarily of sulfuric acid and water with a 75/25 mix of H_2SO_4/H_2O. This assumption impacts the particle size retrieval through the index of refraction, which for background conditions is typically between 1.40 to 1.44, depending on wavelength. If particles are more hydrated this may reduce the index of refraction. To estimate the upper bound of the error due to the assumed index of refraction the retrieval is also performed assuming droplets of pure-water. This leads to retrieved effective radii consistently 100 nm larger than when particles have a H_2SO_4/H_2O mix.

Figure S6(a-g) shows the effective radius retrieved from SAGE III for the months following the HT eruption using the H_2SO_4/H_2O and pure-water compositions in red and blue respectively. Background conditions, shown in dashed lines, typically have an effective radius of approximately 230 nm. After the eruption, particle size increases to over 400-500 nm, depending on composition; larger than at any other point in the SAGE III/ISS record. This growth is contained primarily between 22 and 26 km, which contains the bulk of the enhanced aerosol.

Figure S6h shows aerosol extinction at 755 nm retrieved from OMPS–LP using a tomographic algorithm [5]. The OMPS product shows a clear layer centered at 24.5 km beginning in February. By mid-March the particles have reached their maximum size and this layer begins settling. The

gray line in Figure S6h tracks the peak altitude of the plume. A linear fit to the peak beginning March 10th suggests a settling rate of 0.26 mm/s. This is corrected using the monthly averaged ERA5 vertical wind speed to obtain the fall speed. Ref. [6] estimated the particle size from the fall speed, and applying this formula provides a radius of 350 to 540 nm, depending whether the particle density is typical of background aerosol or pure water. This is shown in Fig. 6i (solid lines) along with the SAGE III/ISS estimates of effective radius (dots). Generally, however these methods produce consistent particle sizes that point to substantial particle growth through condensation and/or coagulation of particles compared to prior eruptions in the SAGE III/ISS period.

Figure S7 shows the retrieved lognormal parameters from the SAGE III/ISS data for October 2021 to June 2022 at various altitude levels. Points are colored by the number of days since the eruption. Before February, values shown as deep purple fall on a well-defined line of near-constant Angstrom exponent, due to the shallow nature of solution space under these conditions. At 25.5 km particle size rapidly increases after the eruption to the largest size by March, then can be seen to relax back to near-background levels. At 24.5 km the enhanced aerosol after the eruption is visible as well-defined mode of distribution parameters that relaxes to particles with a median radius of 300 nm and width of 1.25 by 130 days after the eruption - still considerably elevated over background. At 23.5 km lognormal parameters continue to evolve towards larger, more well-defined particles, although with little change to the effective radius. Below 23 km particle size continues to increase up to 130 days past the eruptions as large particles from higher altitudes sediment and condensation and coagulation processes proceed. Altitudes below 23.5 km also exhibit a larger variation in retrieved parameters, potentially indicating a more complex interplay between the sedimentation, condensation and coagulation processes.

Coagulation processes can both increase or decrease aerosol extinction by changing the scattering efficiency of the particles. Scattering efficiency at 755 nm per volume of aerosol reaches at peak at particles with a radius near 400 nm for typical background conditions, and near 500 nm for purely water. Therefore, coagulation of particles smaller than this will increase extinction while conserving volume. Conversely, collision of very large particles will tend to conserve both volume and extinction as the optical cross section in this case scales approximately with the cube of the radius. The bottom panels in Figure S7 show the correlation between extinction and the aerosol volume computed from the retrieved lognormal distribution. When extinction values are low, the retrieved aerosol volume is sensitive to the particular lognormal parameters, while large volumes tend to be very well correlated with extinction. At 25.5 km the rapid increase in extinction and volume is evident with a subsequent relaxation. 24.5 and 23.5 km are slower to relax with 22.5 km still exhibiting near-peak values 130 days after the eruption.

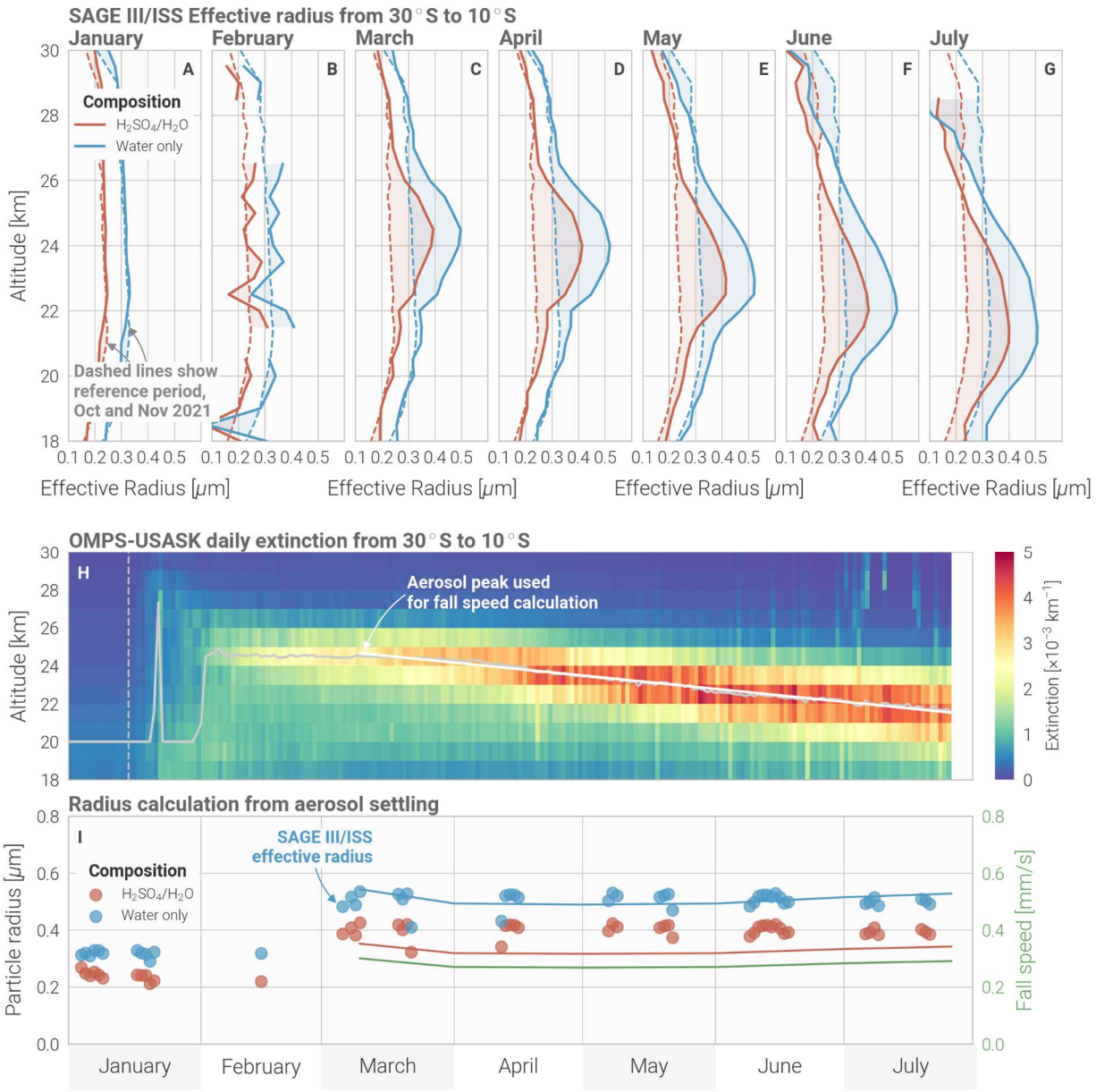

Figure S6. Estimation of particle size from SAGE III/ISS and OMPS-LP. Panels A-G show the monthly averaged retrieved effective radius from SAGE III/ISS assuming background (blue) and pure-water (red) aerosol composition. Dashed lines indicate the average effective radius pre-eruption, computed from October and November 2021 profiles. Panel H shows the daily mean 745 nm aerosol extinction retrieved tomographically from OMPS-LP. The gray line indicates the altitude of the aerosol peak with the white line showing the linear fit. The dashed gray line indicates the eruption date of Hunga-Tonga. Panel I shows the particle radius calculated from the fall speed in blue and red lines for water and H_2SO_4/H_2O compositions respectively. The calculated fall speed is shown in green. Dots indicate the retrieved SAGE III/ISS effective radius at the peak altitude.

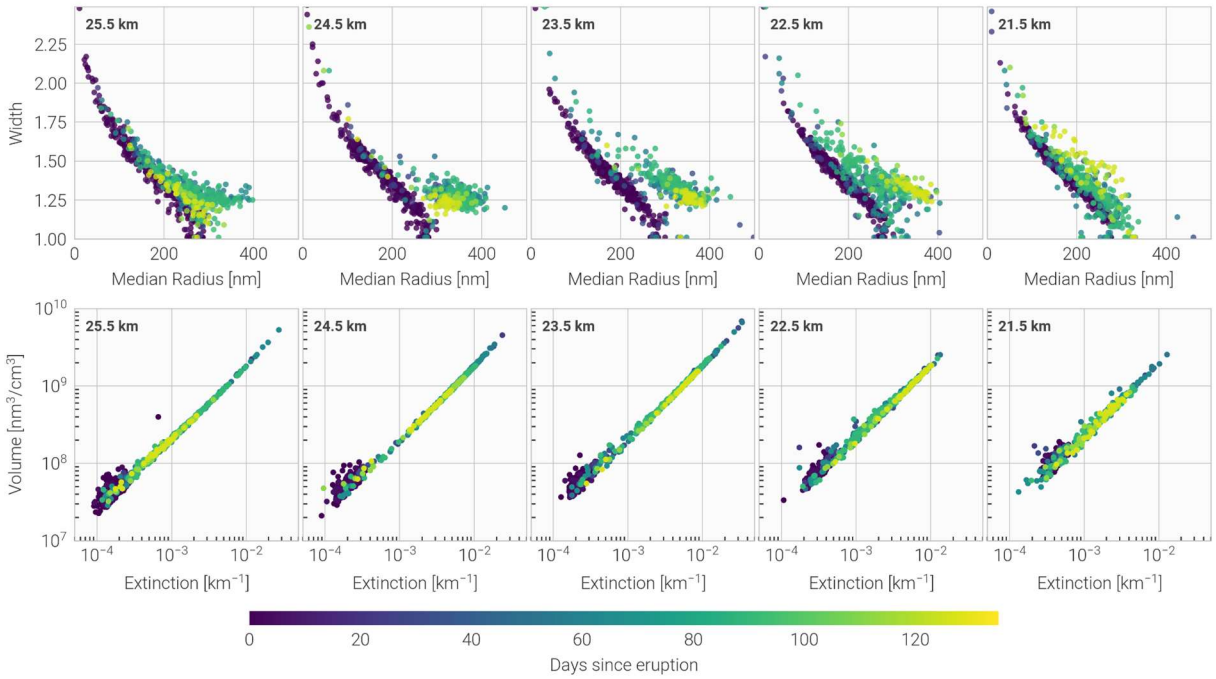

Figure S7. SAGEIII/ISS retrieved aerosol size parameters. Top row shows the retrieved lognormal median radius and width between 21.5 and 25.5 km altitudes. Color indicates the number of days since the Hunga eruption. Bottom row shows the extinction at 755 nm and the retrieved volume computed from the lognormal distribution.

Supplementary notes. S.VI Heavy water isotopologues in the stratosphere from ACE-FTS

Isotopic values are often reported in 'delta' notation, where, for example:

$$\delta D = (1\text{-}R/Rs)*1000,$$

where R is the isotopic ratio in the analyte, Rs is the isotopic ratio in a reference sample (Standard Mean Ocean Water or SMOW in the case of δD), and the factor of 1000 renders the result in units of per mille. A δD value of 0‰ indicates that the analyte has the same isotopic ratio as the standard, and a value of -1000‰ means that isotopic ratio of the analyte is zero.

Vapor phase measurements of δD are useful probes of the atmosphere due to the large fractionation factor of HDO relative to H_2O, especially at the low temperatures found in the upper troposphere and lower stratosphere. The practical effect of HDO's elevated fractionation factor (or, put another way, lower vapor pressure) relative to H_2O is that as moist air ascends, cools, and forms ice particles or water droplets, the heavier isotopologues preferentially partition into the condensed phases, thus depleting the vapor and enriching the condensates. The isotopic difference between vapor and condensate becomes more extreme the colder an air parcel becomes, and indeed the most depleted air in Earth's atmosphere is found in its coldest points, namely Antarctica and the tropical cold point. This effect has been used in studies of tropical convection to understand the average tropical profile of δD, e.g. ref. [7, 8].

Supplementary notes S.VII. Observation of Hunga aerosols by Aeolus ALADIN

Aeolus ALADIN instrument is the first space-borne High Spectral Resolution Lidar (HSRL) instrument for wind and aerosol/cloud profiling in the troposphere and lower stratosphere, operating in orbit since 2018 (see Methods). The vertical range for profiling can be dynamically modified by changing the Range Bin Setting (RBS), which determines the width of atmospheric layers from which the lidar signal is integrated and hence the vertical resolution and the vertical range. Typically, the RBS is configured such that the upper range of profiles is limited to the lower stratosphere, up to 18 - 22 km. However after the Hunga eruption, the RBS was set to reach the altitude of 30 km in order to enable a rare opportunity of wind measurements in the stratosphere using particulate backscatter (Mie) signal as well as to assess the capacity of ALADIN in stratospheric aerosol measurements.

Figure S8 shows a series of monthly-averaged latitude-altitude sections of scattering ratio for the months of January to May 2022. In January, Aeolus captures an intense scattering layer between 25 - 30 km with zonal-mean scattering ratios (SR) at 355 nm up to 5. This is consistent with CALIOP data reporting SR values up to 10 at 532 nm considering the wavelength difference (Figure 1 in ref. 9). In February, the bulk layer of aerosol is found between 24 - 27 km, suggesting gravitational settling of Hunga aerosols. Over the following months, as the plume spreads in the meridional space, the SR decreases to 2 at the zonal-mean scale in agreement with CALIOP 532 nm SR of around 4.

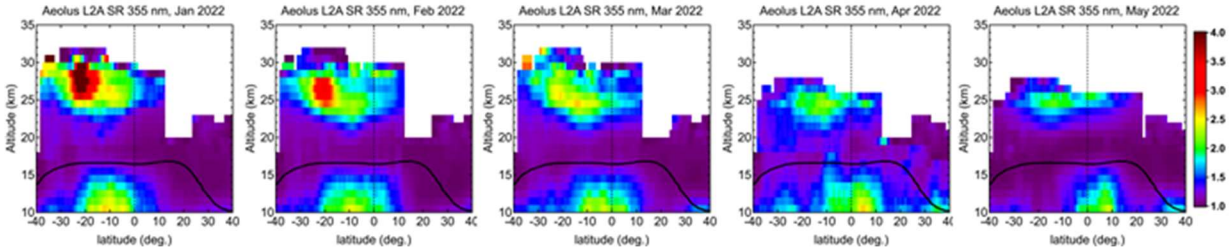

Figure S8. Evolution of the bulk of aerosol in the latitude-altitude space from Aeolus ALADIN satellite lidar. The panels display monthly-averaged scattering ratio (355 nm) for January through March 2022 from ALADIN L2A product. Black curve marks the tropopause level.

Supplementary methods

Ground-based lidars

S.2.1 Atmospheric Physics Observatory of La Réunion

The Maïdo station, as part of the Atmospheric Physics Observatory of La Réunion (OPAR), is located in the South-West Indian Ocean (21°S, 55°E, 2160 m) on the lee side of the Réunion island. The facility [10] hosts since 2013 the LiO3T lidar operating at 532 nm routinely with an average of 8-10 acquisition nights per month. The aerosol optical properties are retrieved at a 50 m vertical resolution following an iterative Klett inversion method with a prior knowledge of i) the molecular backscatter profiles from radiosondes launches and ii) the aerosol optical depth assessed with the Rayleigh slope method in the stratosphere. A more detailed description of the instrument, aerosol retrieval method and error budget are provided by ref. 3 and references therein.

S.2.2 Lauder Atmospheric Research Station

The Lauder Atmospheric Research Station of the National Institute of Water and Atmospheric Research (NIWA) located in South Island of New Zealand (45.0° S, 169.7° E, 370 m) has been operating at 532 nm since 1992 on a regular basis with a mean measurement rate of 1 or 2 nights per week. It has a capability of both scattering ratio and particle depolarization ratio measurements. For retrieving vertical profile of the scattering ratio, we apply Fernald inversion method assuming the aerosol extinction-to-backscatter ratio of 46 sr. The molecular backscattering coefficient is derived from the JRA-55 meteorological analysis. The resulting vertical profiles of aerosol parameters are reported at 150 m vertical resolution. A more detailed description of the instruments, aerosol retrieval and error budget are provided by ref. 11, 12.

S.2.3 Dumont d'Urville station

The French Antarctic station Dumont d'Urville (66.6°S – 140°E, DDU) has hosted an aerosol/cloud lidar since April 1989, operating in the framework of the Network for Detection of Atmospheric Composition Changes (NDACC). The main focus of the instrument is the stud of polar stratospheric clouds with nighttime setup, still, the recent focus on aerosol plumes either originating from volcanic or biomass burning activity extended the measurement calendar to the summertime. The Nd:YAG laser source emits at 532 nm, at 10 Hz frequency with an emitted power of approximately 250 mJ. Backscattered photons are collected on a collocated 80 cm diameter Newton telescope. A polarizing cube at the reception splits the beam into two components polarized parallel and perpendicular to the laser emission for the 532 nm wavelength, each component is recorded and inverted to gain access to the depolarization ratio. The Rayleigh/Mie/Raman lidar also acquires the N2 vibrational Raman scattering at 607 nm. As the OHP lidar, the signal inversion is performed using the Klett-Fernald formalism derive scattering ratio profiles, which have a 60 m vertical resolution. ECMWF meteorological data is also used for the molecular backscattering calculation. A detailed description of the instrument, measurements processing method as well as error estimation is available in ref. 13.

S.2.4 Mauna Loa Observatory

The NOAA Mauna Loa Observatory (19.5° N, 155.6° W, 3396 m a.s.l.) established a Ruby laser-based lidar in the early 1970's which operated until 1998. A Nd:YAG laser-based lidar began operation in 1994. The YAG system operates about once per week and retrieves aerosol profiles at 532 and 1064 nm at 300 m altitude resolution. Molecular profiles needed for analysis are calculated from radiosondes launched at Hilo, HI (56 km distant) and the NASA/MSIS model for

altitudes above the radiosonde. The signal is usually normalized between 38 and 40 km and the Fernald-Klett inversion method is used. A more detailed description can be found in ref. 14.

S.2.5 Tsukuba Meteorological Research Institute

The Meteorological Research Institute (MRI) located at Tsukuba in Japan (36.1° N, 140.1° E, 23 m) is equipped with Mie/Rayleigh lidar for measuring the aerosol between the troposphere and stratosphere. The lidar used in this study is an Nd:YAG lidar system operating at a wavelength of 532 nm, with a capability of both scattering ratio and particle depolarization ratio measurements. The lidar has been operating almost continuously since 2002. For retrieving vertical profile of the scattering ratio, we apply Fernald inversion method assuming the aerosol extinction-to-backscatter ratio of 50 sr. The molecular backscattering coefficient is derived from the collocated radiosonde launched at Aerological Observatory (Tateno) and JRA-55 meteorological analysis. The resulting vertical profiles of aerosol parameters are reported at 150 m vertical resolution. A more detailed description of the instruments, aerosol retrieval and error budget is provided in ref. 12.

S.2.6 Kühlungsborn observatory

The Kühlungsborn RMR lidar is located at the Leibniz Institute for Atmospheric Physics in northern Germany (54.12° N, 11.77° E, 71 m) and measures temperature, horizontal winds, aerosols, and NLCs using a three-beam configuration of one zenith and two off-zenith lines of sight. The lidar operates at 532 nm with N2 vibrational Raman at 608 nm and N2/O2 rotational Raman channels at 529.1 and 530.4 nm (vertical only). The vertical beam is daylight capable and semi-autonomous while the off-zenith beams are operated every clear night. The vertical system has been in operation since 2010 and averages typically 10 acquisitions per month (1000-1400 hours per year). Aerosol Backscatter Ratio is calculated using the nighttime measurements from the 532 nm Rayleigh and 608 nm vibrational Raman channel with MSIS2.0 used as a molecular backscattering reference. The resulting aerosol ratio profiles span 20 to 40+ km with a gridded resolution of 15 m and 30 seconds. A vertical and temporal Savitzky-Golay filter are applied to the data with a final effective resolution of approximately 100 m and 5 minutes. Further system details of the vertical pointing lidar can be found in ref. 15.

S.2.7 Alomar observatory

The Arctic Lidar Observatory for Middle Atmosphere Research (ALOMAR) RMR lidar located in northern Norway (69.16° N, 16.00° E, 380 m) is measuring temperature, horizontal winds, aerosols, and NLCs. The lidar uses two independent off-zenith pointing beams at 1064, 532, and 355 nm with N2 and H2O vibrational Raman and N2/O2 rotational Raman channels at 387, 608, 660, 529.1 and 530.4 nm. The lidar is capable of operating semi-autonomously day and night. The system has been in operation since 1994 and averages about 10 acquisitions (nights and days) per month (800 hours per year). Aerosol Backscatter Ratio and Aerosol Colour Ratio are calculated using ECMWF data to account for Rayleigh and Ozone extinction. Aerosol Extinction profiles are calculated using ECMWF data as molecular reference. The resulting aerosol profiles span ~7 to 40+ km with a gridded resolution of 150 m and 5 minutes. Further system details can be found in ref. 16.

S.2.8 Haute-Provence Observatory

The Observatoire de Haute-Provence (OHP) located in southern France (43.9° N, 5.7° E, 670 m) is equipped with several lidar systems for atmospheric sounding at a wide range of altitudes. The aerosol measurements are provided by LTA lidar operating at 532 nm since 1991 on a regular basis with a mean measurement rate of 10-12 acquisition nights per month. For retrieving vertical profiles of stratospheric aerosol, we apply Fernald-Klett inversion method, which provides

backscatter and extinction coefficients. The scattering ratio is then computed as a ratio of total (molecular plus aerosol) to molecular backscattering, where the latter is derived from ECMWF meteorological analysis. The resulting vertical profiles of aerosol parameters are reported at 150 m vertical resolution. A more detailed description of the instruments, aerosol retrieval and error budget are provided in ref. 17 and references therein.

Supplementary references

1. Millán, L., Santee, M. L., Lambert, A., Livesey, N. J., Werner, F., Schwartz, M. J., et al. (2022). The Hunga Tonga-Hunga Ha'apai Hydration of the Stratosphere. Geophysical Research Letters, 49, e2022GL099381. https://doi.org/10.1029/2022GL099381
2. Sellitto, P., Podglajen, A., Belhadji, R. et al. The unexpected radiative impact of the Hunga Tonga eruption of 15th January 2022. Commun Earth Environ 3, 288 (2022). https://doi.org/10.1038/s43247-022-00618-z, 2022
3. Baron A., P. Chazette, S.Khaykin, G. Payen, N. Marquestaut, N. Bègue and V. Duflot. Early Evolution of the Hunga-Tonga Aerosol Stratospheric Plume from Lidar Observations at La Réunion, Submitted to Geophys. Res. Lett., 2022, https://doi.org/10.1002/essoar.10512319.1
4. Xu, J.; Li, D.; Bai, Z.; Tao, M.; Bian, J. Large Amounts of Water VaporWere Injected into the Stratosphere by the Hunga Tonga–Hunga Ha'apai Volcano Eruption. Atmosphere 2022, 13, 912. https://doi.org/10.3390/atmos13060912
5. Zawada, D. J., Rieger, L. A., Bourassa, A. E., and Degenstein, D. A.: Tomographic retrievals of ozone with the OMPS Limb Profiler: algorithm description and preliminary results, Atmos. Meas. Tech., 11, 2375–2393, https://doi.org/10.5194/amt-11-2375-2018, 2018
6. Kasten
7. Moyer, E. J., Irion, F. W., Yung, Y. L., and Gunson, M. R.: ATMOS stratospheric deuterated water and implications for troposphere-stratosphere transport, Geophys. Res. Lett., 23, 2385–2388, 1996, https://doi.org/10.1029/96GL01489
8. Khaykin, S. M., Moyer, E., Krämer, M., et al..: Persistence of moist plumes from overshooting convection in the Asian monsoon anticyclone, Atmos. Chem. Phys., 22, 3169–3189, https://doi.org/10.5194/acp-22-3169-2022, 2022.
9. Legras, B., Duchamp, C., Sellitto, P., Podglajen, A., Carboni, E., Siddans, R., Grooß, J.-U., Khaykin, S., and Ploeger, F.: The evolution and dynamics of the Hunga Tonga plume in the stratosphere, EGUsphere [preprint], https://doi.org/10.5194/egusphere-2022-517, 2022
10. Baray, J.-L., Courcoux, Y., Keckhut, P., Portafaix, T., Tulet, P., Cammas, J.-P., Hauchecorne, A., Godin Beekmann, S., De Mazière, M., Hermans, C., Desmet, F., Sellegri, K., Colomb, A., Ramonet, M., Sciare, J., Vuillemin, C., Hoareau, C., Dionisi, D., Duflot, V., Vérèmes, H., Porteneuve, J., Gabarrot, F., Gaudo, T., Metzger, J.-M., Payen, G., Leclair de Bellevue, J., Barthe, C., Posny, F., Ricaud, P., Abchiche, A., and Delmas, R.: Maïdo observatory: a new high-altitude station facility at Reunion Island (21° S, 55° E) for long-term atmospheric remote sensing and in situ measurements, Atmos. Meas. Tech., 6, 2865–2877, https://doi.org/10.5194/amt-6-2865-2013, 2013
11. Nagai, T., Liley, B., Sakai, T., Shibata, T., and Uchino, O.: PostPinatubo evolution and subsequent trend of the stratospheric aerosol layer observed by mid-latitude lidars in both hemispheres, SOLA, 6, 69–72, doi:10.2151/sola.2010-018, 2010
12. Sakai, T., O. Uchino, T. Nagai, B. Liley, I.Morino, and T. Fujimoto (2016), Long-term variation of stratospheric aerosols observed with lidars over Tsukuba, Japan, from 1982 and

Lauder, New Zealand, from 1992 to 2015, J. Geophys. Res. Atmos., 121, 10,283 – 10,293, doi:10.1002/2016JD025132
13. Tence F., Jumelet J., Bekki S., Khaykin S., Sarkissian A., Keckhut P., Australian Black Summer smoke observed by lidar at the French Antarctic station Dumont d'Urville, Journal of Geophysical Research: Atmospheres, American Geophysical Union, 2022, 127 (4), pp.e2021JD035349. ⟨10.1029/2021JD035349⟩
14. Barnes, J. E., and D. J. Hofmann, Lidar measurements of stratospheric aerosol over Mauna Loa Observatory, Geophys. Res. Lett., 24, 1923-1926, 1997.
15. Gerding, M., Kopp, M., Höffner, J., Baumgarten, K., and Lübken, F.-J.: Mesospheric temperature soundings with the new, daylight-capable IAP RMR lidar, Atmos. Meas. Tech., 9, 3707–3715, https://doi.org/10.5194/amt-9-3707-2016, 2016.
16. Baumgarten, G.: Doppler Rayleigh/Mie/Raman lidar for wind and temperature measurements in the middle atmosphere up to 80 km, Atmos. Meas. Tech., 3, 1509–1518, https://doi.org/10.5194/amt-3-1509-2010, 2010.
17. Khaykin, S. M., Godin-Beekmann, S., Keckhut, P., Hauchecorne, A., Jumelet, J., Vernier, J.-P., Bourassa, A., Degenstein, D. A., Rieger, L. A., Bingen, C., Vanhellemont, F., Robert, C., DeLand, M., and Bhartia, P. K.: Variability and evolution of the midlatitude stratospheric aerosol budget from 22 years of ground-based lidar and satellite observations, Atmos. Chem. Phys., 17, 1829–1845, https://doi.org/10.5194/acp-17-1829-2017, 2017

Supplementary Movie S1. Cloud top height 10-minute sequence from stereoscopic retrieval using GOES-17 and Himawari-8 geostationary satellite imagers.

Supplementary Movie S1. CLaMS daily sequence of hydrated plume evolution at 21 hPa pressure level.